Theory of ion holes in space and astrophysical plasmas

Harikrishnan Aravindakshan [ORCID],[1]⋆ Peter H. Yoon,[2,3,4] Amar Kakad[1] and Bharati Kakad[1]

[1]*Indian Institute of Geomagnetism, New Panvel, Navi Mumbai 410218, India*
[2]*Institute for Physical Science and Technology, University of Maryland, College Park, MD 20742, USA*
[3]*School of Space Research, Kyung Hee University, Yongin, South Korea*
[4]*Korea Astronomy and Space Science Institute, Daejeon, South Korea*

ABSTRACT

Coherent bipolar electric field structures, ubiquitously found in various space and astrophysical plasma environments, play an important role in plasma transport and particle acceleration. Most of the studies found in the literature about them pertain to bipolar structures with positive potentials interpreted in terms of electron holes. Magnetospheric Multiscale spacecraft have recently observed a series of coherent electric field structures with negative potential in the Earth's bow shock region, which are interpreted as ion holes. The existing theoretical models of ion holes are inadequate because they entail stringent conditions on the ratio of ion to electron temperature. This letter presents a new theory that provides a satisfactory explanation to these observations. A salient point is that this letter incorporates the electron dynamics in the theoretical formalism, which removes ambiguities associated with existing theories, thus showing that the new theory for ion holes may be widely applicable for space and astrophysical plasmas.

Key words: acceleration of particles – plasmas – turbulence – waves – methods: analytical.

1 INTRODUCTION

The coherent bipolar electric field structures featuring positive or negative monopolar wave potential are ubiquitously observed in space and astrophysical plasmas (Boström et al. 1988; Matsumoto et al. 1994; Mangeney et al. 1999; McFadden et al. 2003; Shin et al. 2008; Hashimoto et al. 2010; Malaspina et al. 2013; Liemohn et al. 2014; Pickett et al. 2015; Kakad et al. 2016; Goodrich et al. 2018; Vasko et al. 2018; Wang et al. 2020). These structures have spatial scales of a few Debye lengths and are known as one of the elements responsible for electrostatic turbulence in the space and astrophysical plasmas. Also, they are important for plasma particle transport and heating. The motion of charged particles trapped in the wave potential can be visualized as bound closed orbits with low density at the centre of the peak wave potential; hence, these structures are known as phase-space holes or vortices. Depending on the trapped particles, they are known as electron phase-space holes, or simply electron holes, or ion phase-space holes or ion holes (Eliasson & Shukla 2006; Aravindakshan, Kakad & Kakad 2018b). Generally, positive potentials are associated with electron holes, while ion holes are associated with negative potentials. Such coherent potentials have been observed in the near-Earth as well as astrophysical plasma environments, but, in general, electron holes are far more common than ion holes (Mangeney et al. 1999; Shin et al. 2008; Hashimoto et al. 2010; Malaspina et al. 2013; Liemohn et al. 2014; Pickett et al. 2015). Signatures of ion holes were first detected only in the late 1980s by the Viking satellite (Boström et al. 1988). Later, more frequent measurements were made by the FAST satellite in the 2000s (McFadden et al. 2003).

The primary aim of the recently launched NASA's Magnetospheric Multiscale (MMS) mission is the investigation of electron-scale phenomena in the magnetic reconnection site. Recently, Vasko et al. (2018) observed intense electrostatic solitary waves with negative monopolar potentials in the supercritical quasi-perpendicular Earth's bow shock crossing by MMS. Later, Wang et al. (2020) analysed the MMS data for the events corresponding to quasi-perpendicular supercritical Earth's bow shock crossing, and proceeded to show that the observed solitary waves are ion Bernstein–Greene–Kruskal (BGK) holes.

Fig. 1 shows observation from the MMS spacecraft on 2017 November 2 around 06:03 UT, which was initially reported by Wang et al. (2020). The top and middle panels, respectively, show the three components of magnetic and electric fields. The zoomed-in view of the 80 ms electric field data after 06:05:0.17 UT is shown in the lower panel. It is seen that the E_z field has a much higher amplitude than the other two
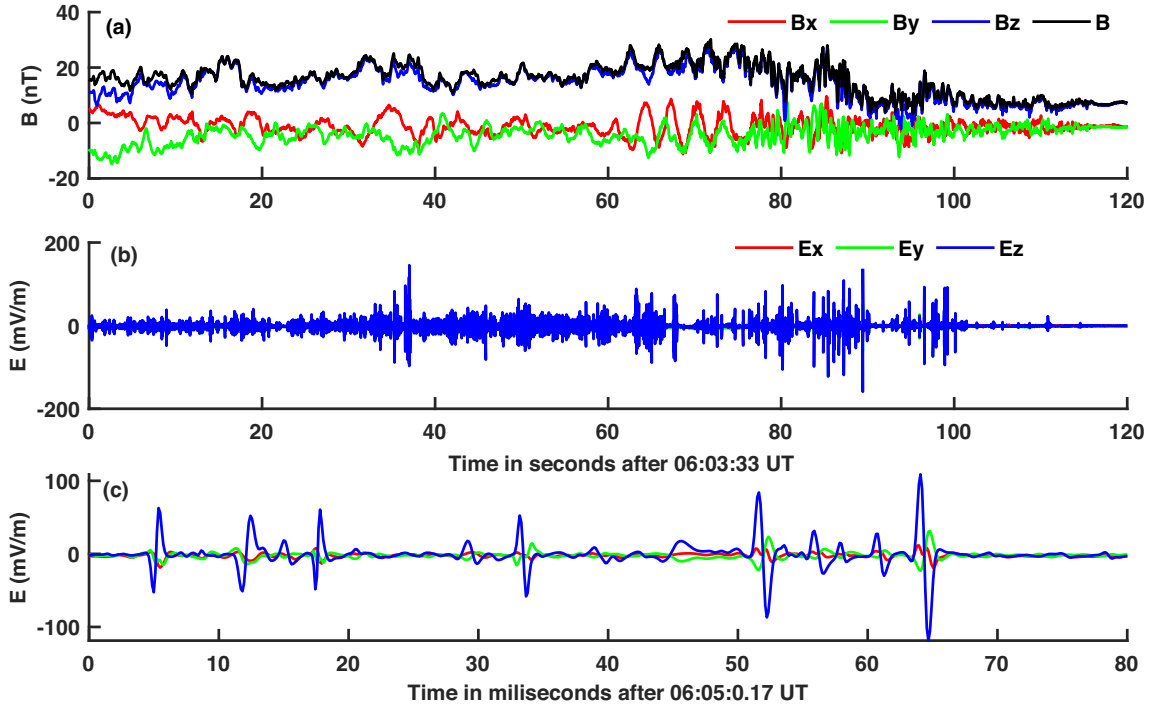
Figure 1. (a) The magnitude of quasi-static magnetic field (*B*) along with three magnetic field components (B_x, B_y, and B_z) and (b) three components of electric field observed by MMS4 spacecraft on 2017 November 2 around 06:03:33 UT. (c) The zoomed view of the electric field data for 80 ms after 06:05:0.17 UT. Here, E_z is the electric field component parallel to the local quasi-static magnetic field, while E_x and E_y are corresponding perpendicular components.

components, which indicates that these are essentially 1D structures. In addition, Wang et al. (2020) mention that the potentials associated with these fields are negative and hence represent ion holes.

The theory of electron phase-space holes is well known. Beginning with the work by Bernstein, Greene & Kruskal (1957), the so-called BGK equilibrium theory solves for the trapped particle distribution function from the steady-state Vlasov equation, and arrives at the possible combination of width and amplitude of the assumed electrostatic potential (Chen 2002; Aravindakshan, Kakad & Kakad 2018a; Aravindakshan et al. 2018b). The theory of ion holes, on the other hand, has attracted far less attention in the literature (Schamel 1971; Bujarbarua & Schamel 1981). The theoretical model for ion holes was introduced by Schamel about half a century ago (Schamel 1971; Bujarbarua & Schamel 1981), but since then not much progress has been made. In view of the recent observations such as those by Wang et al. (2020), it is timely to revisit the theory of ion phase-space holes. As will be explained, the theory of Schamel (1971) is not commensurate with the observed parameters, which provides a further motivation to carry out this work. It is the purpose of this letter to report a more satisfactory theory of ion holes.

Schamel's approach assumes the model of distribution function for trapped particles, and arrives at the solution for electrostatic potential, by essentially solving an eigenvalue problem. This approach, however, appears to be inherently limited to moderate amplitude solutions. Both BGK and Schamel's methods agree on the minimum hole size, but the methods seem to diverge on the maximum allowable hole length in phase space. There is no mathematical limit on the hole length unless additional constraints on the distribution *f* are enforced, but physical ambiguity arises in the Schamel's approach, which effectively leads one to enforce the limitation after all. This is being discussed in detail by Hutchinson (2017) in the context of the electron hole. Among the consequences of the limitation inherent in Schamel's approach is that the theory limits the ion to electron temperature ratio to $T_i/T_e < 0.3$ in order for the ion holes to form (Schamel 1971, 1982). However, this condition is at variance with the latest observation by Wang et al. (2020), as they report $T_i/T_e \sim 0.4$.

An attempt was made by Chen, Thouless & Tang (2004) to develop a theory for BGK equilibrium that encompasses both ion and electron holes. However, upon a close examination of their theory, it is seen that the treatment of the species, which is not part of the dynamics of the hole, is ambiguous. In the case of electron holes, the ions do not impart any considerable effect; however, their model predicts otherwise. Besides, their model predicts that the allowed parameter space for ion and electron holes remains the same, which is highly improbable, as the role of electrons being vital in the ion frame (and vice versa) is not valid. These issues have prompted us to revisit the problem and formulate the ion hole solution on the basis of the classical BGK approach, which has not been done. It should be noted that the BGK ion hole solution is not a trivial extension of the BGK electron hole solution. This is because in the case of BGK electron holes, the ions are considered as an immobile neutralizing background. In contrast, in the case of ion BGK holes, the electrons must be treated as adiabatic. In this way, both electrons and ions must be taken into account.

For the sake of generality, we assume that both electron and ion distributions are specified by kappa models. Spacecraft observations show that the space plasma is characterized by non-thermal features, which are adequately modelled by the kappa distribution. The kappa

distribution may also imply that the space plasma may be governed by non-extensive statistical mechanical principles – see e.g. the monograph by Livadiotis (2017). The non-extensive statistical concept may be equivalent to quasi-equilibrium turbulent state, as recently suggested by Yoon (2019b). For further technical details on plasma turbulence theory, see the recent monograph by Yoon (2019a). Recently, Davis et al. (2019) argue that if a plasma system is in a steady-state collisionless mode, the particles in the system will only follow superstatistics, which leads to the kappa distribution. In short, adopting the kappa model is consistent with data and various theories.

2 THEORETICAL FORMALISM

We begin the discourse based upon a 1D Vlasov–Poisson system of equations that governs the dynamics of ion distribution function f_i in collisionless unmagnetized plasma and adiabatic electrons,

$$\left(\frac{\partial}{\partial t} + V_i \frac{\partial}{\partial x} - \frac{q_i}{m_i} \frac{\partial \Phi}{\partial x} \frac{\partial}{\partial V_i} \right) f_i = 0, \tag{1}$$

$$\frac{d^2 \Phi}{dx^2} = -\frac{(q_e N_e + q_i N_i)}{\epsilon_0}, \tag{2}$$

where f_i, q_i, V_i, and m_i denote the distribution function, charge, velocity, and mass of ions, respectively. Here, $q_e = -e$ for electrons and $q_i = +e$ for ions. N_e and N_i are electron and ion densities such that $N_e = N_i = N_0$. Φ is the electrostatic potential and ϵ_0 is the vacuum permittivity. It is convenient to work in a coordinate system in which the ion hole is at rest so that all quantities are time independent. In such a case, equations (1) and (2) reduce to the following normalized form:

$$v \frac{\partial f_i(v, x)}{\partial x} + \frac{1}{2} \frac{\partial \phi}{\partial x} \frac{\partial f_i(v, x)}{\partial v} = 0, \tag{3}$$

$$\frac{d^2 \phi}{dx^2} = n_e - n_i. \tag{4}$$

In this letter, we assume that the charged particle velocity distribution functions are given by kappa models for reasons discussed above.

In equation (4), we have made use of the definition $n_i = \int_{-\infty}^{\infty} f_i(x, v) dv$, and n_e is the electron density, which can be obtained by taking the first moment of the 1D kappa velocity distribution function (Saini, Kourakis & Hellberg 2009; Lotekar, Kakad & Kakad 2016):

$$n_e = \left(1 - \frac{\phi T_r}{\kappa_e - (3/2)} \right)^{-\kappa_e + (1/2)}. \tag{5}$$

Here, $T_r = T_i/T_e$ is the ion to electron temperature ratio, and κ_e denotes the suprathermal index of adiabatic electrons. In equation (3), v is the normalized ion velocity in the frame comoving with the wave perturbation. The normalizations are such that x is normalized by the ion Debye length $\lambda_{di} = \sqrt{k_B T_i / \epsilon_0 N_0 e^2}$, velocity is normalized with ion thermal velocity $v_{th,i} = \sqrt{2k_B T_i / m_i}$, and ϕ is the potential normalized by $k_B T_i / e$. Here, T_i is the ion temperature, k_B is the Boltzmann constant, and N_0 is the equilibrium density of electrons. We consider suprathermal ions in the model that follow the kappa distribution.

The normalized form of ion distribution function is given by

$$f_i(v) = \frac{\Gamma(\kappa_i)}{\pi^{(1/2)} \Gamma(\kappa_i - (1/2)) (\kappa_i - (3/2))^{(1/2)}} \left(1 + \frac{v^2}{\kappa_i - (3/2)} \right)^{-\kappa_i}. \tag{6}$$

Here, κ_i denotes the suprathermal index of ions. Let us write the ion distribution function in terms of the normalized total energy of the particles:

$$w = \frac{1}{2} \left(v^2 + \phi \right). \tag{7}$$

Consequently, equation (6) transforms as

$$f_i(w) = \frac{\Gamma(\kappa_i)}{\pi^{(1/2)} \Gamma(\kappa_i - (1/2)) (\kappa_i - (3/2))^{(1/2)}} \left(1 + \frac{2w - \phi}{\kappa_i - (3/2)} \right)^{-\kappa_i}, \tag{8}$$

where $f(x, v) dv = f(w) dw / \sqrt{2w - \phi}$.

We assume a Gaussian negative potential form, which is supported by spacecraft observations in the Earth's magnetosphere, where such a Gaussian wave potential structure is shown to be quite common:

$$\phi(x) = -\psi \exp \left(-\frac{x^2}{2\delta^2} \right), \tag{9}$$

where ψ represents the amplitude and δ is the width of the perturbation. Note that δ signifies a distance at which the potential decreases to 0.6065ψ. The full width at half-maximum of the perturbation is given by $\Delta = 2.35\delta$ (Aravindakshan et al. 2018a).

As there are two kinds of ion population, trapped and passing, we distinguish the passing particle distribution function by f_p and the trapped particles by f_{tr}. We assume that all ions have same velocity such that when we move into the ion frame, and derive the expression for holes, all of them have same velocity.

The net charge density is made of combined passing (n_p) and trapped (n_{tr}) charged densities. As a consequence, equation (4) is written as

$$\frac{d^2\phi}{dx^2} = n_e - n_p - n_{tr}. \tag{10}$$

Integrating the passing ion distribution function under the proper limits, we obtain the passing ion density

$$n_p = 1 - \frac{2A\sqrt{-\phi}}{\sqrt{B}} \, {}_2F_1\left(\kappa_i, \tfrac{1}{2}, \tfrac{3}{2}; \frac{\phi}{B}\right), \tag{11}$$

where ${}_2F_1(a, b, c; z)$ is the hypergeometric function, and

$$A = \frac{\Gamma(\kappa_i)}{\pi^{(1/2)}\Gamma(\kappa_i - (1/2))} \quad \text{and} \quad B = \kappa_i - \frac{3}{2}. \tag{12}$$

Making use of equation (11) for passing ion density, we obtain the trapped ion density

$$n_{tr} = \left(\frac{\rho T_r}{\kappa_e - (3/2)} + 1\right)^{(1/2)-\kappa_e} - \frac{2\rho \log(\rho/\psi)}{\delta^2} - \frac{\rho}{\delta^2} - 1 + \frac{2A\sqrt{\rho}}{\sqrt{B}} \, {}_2F_1\left(\kappa_i, \tfrac{1}{2}, \tfrac{3}{2}; -\frac{\rho}{B}\right). \tag{13}$$

Making use of the trapped ion density, equation (13), we may construct the trapped ion distribution function (f_{tr}). The method closely follows those by Chen (2002) and Aravindakshan et al. (2018a). The result is as follows:

$$f_{tr}(w) = \frac{A}{\sqrt{B}} \, {}_2F_1\left(\tfrac{1}{2}, \kappa_i; 1; \frac{2w}{B}\right) - \sqrt{-w}\left\{0.9T_r\frac{\kappa_e - (1/2)}{\kappa_e - (3/2)} \, {}_2F_1\left(1, \kappa_e + \tfrac{1}{2}; \tfrac{3}{2}; \frac{4T_r w}{2\kappa_e - 3}\right)\right.$$
$$\left. + \frac{4\sqrt{2}}{\pi\delta^2}\left[\log\left(-\frac{8w}{\psi}\right) - \tfrac{1}{2}\right]\right\}. \tag{14}$$

The trapped ion distribution function in equation (14) consists of three significant terms that are crucial for self-sustainable ion BGK equilibrium. The first term on the right-hand side stems from the ion contribution. As this is the only positive definite term, and the trapped ion distribution function should be positive in order to represent a physical scenario, this term is exclusively responsible for the physical plausibility of the developed ion holes. The next term on the right-hand side of the equality is negative, and is inherently composed of two terms enclosed within large curly brackets. As these two terms are negative, they contribute towards the distortion of ion BGK equilibrium. The second term within the large curly brackets shows the effects of total charge density in the formation of BGK equilibria. The first term, in contrast, manifests the role of electrons, which contributes to the destruction of ion BGK equilibria depending on the plasma condition. When the temperature ratio increases to the extent that the ion temperature becomes lower than the electron temperature, the electron density interacts with the equilibria in such a way that the trapped ion distribution function becomes discontinuous and engages in the distortion of the generated equilibria. Such a mechanism is prohibited in the model by Chen et al. (2004).

In order for the ion trapped distribution (14) to represent physically meaningful stable equilibria of ion holes, we require that $f_{tr}(w)$ is always positive. Employing this criterion, we arrive at an inequality governing the width and amplitude of the wave potential ,

$$\delta^2 \geq \frac{4\sqrt{2}\sqrt{-w}\left[\log(-(8w/\psi)) - (1/2)\right]}{0.9\pi \, T_r\sqrt{-w}\,(\kappa_e - (1/2))/(\kappa_e - (3/2)) \, {}_2F_1\left(1, \kappa_e + (1/2); (3/2); (4T_r w)/(2\kappa_e - 3)\right) + \pi A\sqrt{B} \, {}_2F_1\left((1/2), \kappa_i; 1; (2w/B)\right)}. \tag{15}$$

Inequality (15) places constraints on the width and amplitude associated with the wave potential that supports the ion holes. Fig. 2 depicts the region of validity in the $(-\psi, \delta)$ parametric space as the suprathermal index κ and ion to electron temperature ratio T_r are varied. The top panels represent the case of highly suprathermal plasma ($\kappa_i = \kappa_e = 2$), and the bottom panels represent the case of nearly thermal plasma ($\kappa_i = \kappa_e = 200$). The panels on the right-hand side (left-hand side) show the case with temperature ratio $T_r = 0.1$ ($T_r = 3$). The highlighted region (in blue) depicts physically meaningful parameter space, while the white area represents the forbidden region. The choice of $T_r = 3$ highlights the fact that in our model there is no theoretical limitation on the temperature ratio for the generation of ion BGK holes. That is, any arbitrary choice of the temperature ratio can be made, but as can be seen in Fig. 2, high values of T_r can place a significant limit on the region of validity in the $(-\psi, \delta)$ phase space. As the ion temperature exceeds the electron temperature ($T_r > 1$), the forbidden region increases. It is interesting to note that, for given value of T_r, the region of validity is noticeably wider for the Maxwellian case ($\kappa_i = \kappa_e = 200$) than for the non-thermal case ($\kappa_i = \kappa_e = 2$). In short, Fig. 2 serves the purpose of illustrating that our model has no inherent limitation on the temperature ratio $T_r = T_i/T_e$, and also the importance of thermal electrons in controlling the region of validity in the $(-\psi, \delta)$ parameter space.

3 APPLICATION TO MMS OBSERVATIONS

In order to demonstrate the usefulness of this theory, we return to Fig. 1, which is an independent analysis of the MMS observations of ion holes first discussed by Wang et al. (2020). As noted previously, Wang et al. (2020) report that $T_r = T_i/T_e$ is approximately 0.4, which is beyond the region of validity according to Schamel (1971, 1982), but is valid in the context of our theory. Solving equation (15) for $T_r = 0.4$, we plotted the physically plausible region of ion BGK equilibria in Fig. 3. As the ion hole observations are from the bow shock region, which is constantly perturbed by the solar wind plasma, we have assumed the distribution of both electrons and ions to be highly non-thermal ($\kappa_e = \kappa_i = 2$) (Gosling et al. 1989; Pierrard & Lazar 2010; Gedalin & Dröge 2013; Livadiotis 2017). During this event, Wang et al. (2020)
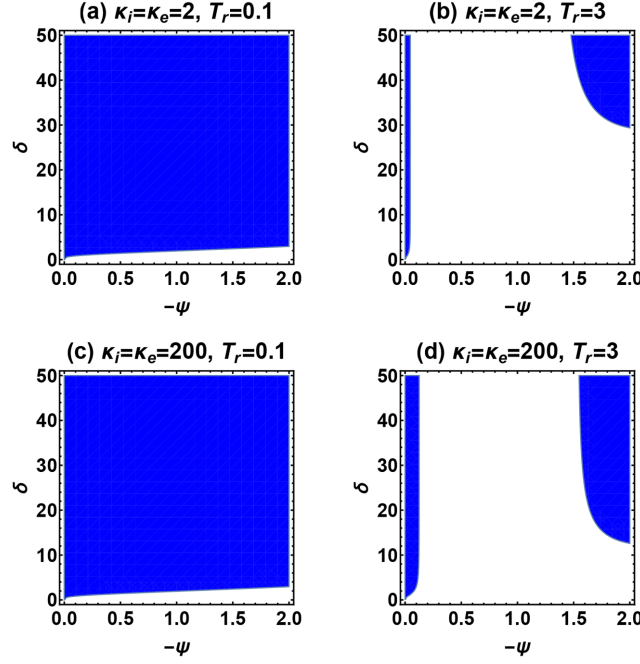
Figure 2. Physically plausible region of ion BGK equilibria in the $(-\psi, \delta)$ phase space for different κ and T_r is displayed. If the generated potential has width and amplitude from the shaded region (displayed in blue), the resultant wave potential can support stable ion BGK equilibria.
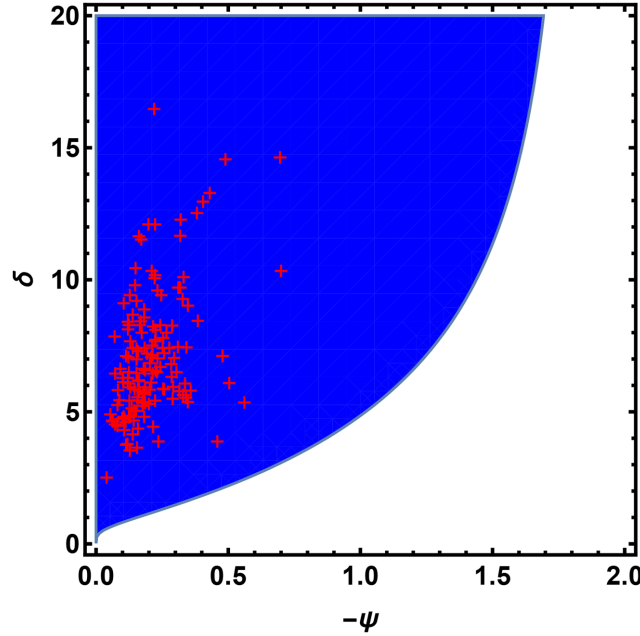
Figure 3. The width and amplitude of all the observed ion holes (shown with `+' symbols) are superimposed on the physically allowed regions predicted by our theoretical model, with the observed value of temperature ratio ($T_r = 0.4$). This figure exemplifies that the developed theoretical model is on a par with the observations.

reported about 134 ion holes. Fig. 3 shows the MMS observations of all 134 holes (shown with `+' symbols) in the $(-\psi, \delta)$ parameter space, which indicates that all data points are well within the region of validity. As Fig. 2 shows, the physically plausible parameter space supported by thermal plasma is broader than that for suprathermal plasma. Consequently, our interpretation of observations in the context of ion BGK solutions, as depicted in Fig. 3, applies a fortiori, if we adopt thermal distributions.

Furthermore, we obtained the trapped ion distribution function and its corresponding phase-space portrait of the largest ion hole with peak potential $\phi = -3.5$ V and width 32 m observed by Wang et al. (2020) as shown in Fig. 4. The observed potential and the width converted as per the normalization used in our theory. The suprathermal index of both ions and electrons is assumed to be $\kappa_i = \kappa_e = 2$ and the temperature ratio $T_r = 0.4$. The horizontal axes (x, v) represent normalized spatial coordinate and velocity. The yellow colour scheme
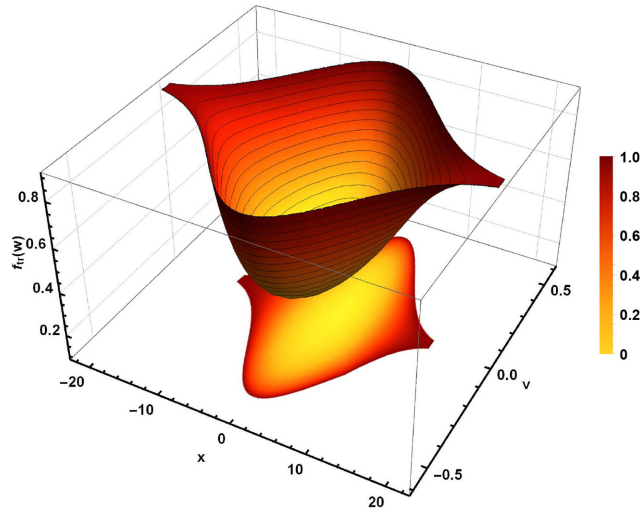
Figure 4. The phase-space portrait of trapped distribution of the largest ion hole reported by Wang et al. (2020). The projection of the trapped particle distribution on to the (x, v) plane is superposed to visualize the phase-space structure of the ion hole. The amplitude of the potential is $\psi = -0.25\ (= -3.5\ \text{V})$ and width $\delta = 6.32\ (32\ \text{m})$, as observed by MMS with the background ion to electron temperature ratio of 0.4.

shows the region of low ion density, while the darker red colour map indicates the region of high density. The projection of the trapped ion distribution on to the (x, v) plane is also superposed in order to aid visual identification of the phase-space structure.

4 CONCLUSION

To conclude, this letter reports the formulation of BGK theory of ion holes that is uniformly valid for all ion to electron temperature ratio T_i/T_e. This problem has been partly motivated by the recent (as well as past) satellite mission that reports ion hole structures, and yet no satisfactory theory is available. This theoretical model shows that the role of electrons in the case of ion holes is inevitable and plays a significant role in their generation. The existing theories (Schamel 1971, 1982) are ineffective in that observed parameters fall outside the region of validity according to such a theory. In contrast, the present theory is uniformly valid, which we have tested against actual space observations. Coherent bipolar electric field structures may play an important role in plasma transport and particle heating. This can be seen from equation (13), which shows that the trapped particle density increases as the temperature ratio increases. This implies a bunch of charged particles trapped in such structures comoving with the bulk speed of the large-amplitude potentials. These fast-moving charged particles may radiate electromagnetic waves, which may subsequently lead to the particle acceleration and heating. These physical processes are beyond the scope of this letter, but the significance of this work is that we have presented a novel theory that may be applicable to any coherent negative potential structures in space and astrophysical plasma.

DATA AVAILABILITY

The MMS spacecraft data underlying this article are publicly available at https://lasp.colorado.edu/mms/public. The derived data generated in this research will be shared on reasonable request to the corresponding author.

REFERENCES

Aravindakshan H., Kakad A., Kakad B., 2018a, Phys. Plasmas, 25, 052901
Aravindakshan H., Kakad A., Kakad B., 2018b, Phys. Plasmas, 25, 122901
Bernstein I. B., Greene J. M., Kruskal M. D., 1957, Phys. Rev., 108, 546
Boström R., Gustafsson G., Holback B., Holmgren G., Koskinen H., Kintner P., 1988, Phys. Rev. Lett., 61, 82
Bujarbarua S., Schamel H., 1981, J. Plasma Phys., 25, 515
Chen L.-J., 2002, PhD thesis, Univ. Washington
Chen L.-J., Thouless D. J., Tang J.-M., 2004, Phys. Rev. E, 69, 055401
Davis S., Avaria G., Bora B., Jain J., Moreno J., Pavez C., Soto L., 2019, Phys. Rev. E, 100, 023205

Eliasson B., Shukla P. K., 2006, Phys. Rep., 422, 225

Gedalin M., Dröge W., 2013, Front. Phys., 1, 29

Goodrich K. A. et al., 2018, J. Geophys. Res.: Space Phys., 123, 9430

Gosling J., Thomsen M., Bame S., Russell C., 1989, J. Geophys. Res.: Space Phys., 94, 10011

Hashimoto K. et al., 2010, Geophys. Res. Lett., 37, L19204

Hutchinson I. H., 2017, Phys. Plasmas, 24, 055601

Kakad A., Kakad B., Anekallu C., Lakhina G., Omura Y., Fazakerley A., 2016, J. Geophys. Res.: Space Phys., 121, 4452

Liemohn M. W., Johnson B. C., Fränz M., Barabash S., 2014, J. Geophys. Res.: Space Phys., 119, 9702

Livadiotis G., 2017, Kappa Distributions: Theory and Applications in Plasmas. Elsevier, Amsterdam

Lotekar A., Kakad A., Kakad B., 2016, Phys. Plasmas, 23, 102108

McFadden J., Carlson C., Ergun R., Mozer F., Muschietti L., Roth I., Moebius E., 2003, J. Geophys. Res.: Space Phys., 108, 8018

Malaspina D. M., Newman D. L., Willson L. B., III, Goetz K., Kellogg P. J., Kerstin K., 2013, J. Geophys. Res.: Space Phys., 118, 591

Mangeney A. et al., 1999, Ann. Geophys., 17, 307

Matsumoto H., Kojima H., Miyatake T., Omura Y., Okada M., Nagano I., Tsutsui M., 1994, Geophys. Res. Lett., 21, 2915

Pickett J., Kurth W., Gurnett D., Huff R., Faden J., Averkamp T., Píša D., Jones G., 2015, J. Geophys. Res.: Space Phys., 120, 6569

Pierrard V., Lazar M., 2010, Sol. Phys., 267, 153

Saini N., Kourakis I., Hellberg M., 2009, Phys. Plasmas, 16, 062903

Schamel H., 1971, Plasma Phys., 13, 491

Schamel H., 1982, Phys. Scr., 1982, 228

Shin K., Kojima H., Matsumoto H., Mukai T., 2008, J. Geophys. Res.: Space Phys., 113, A03101

Vasko I. et al., 2018, Geophys. Res. Lett., 45, 5809

Wang R. et al., 2020, ApJ, 889, L9

Yoon P. H., 2019a, Classical Kinetic Theory of Weakly Turbulent Nonlinear Plasma Processes. Cambridge Univ. Press, Cambridge

Yoon P. H., 2019b, Entropy, 21, 820

This paper has been typeset from a TEX/LATEX file prepared by the author.